Title

Modeling the structural distortion and magnetic ground state of the polar lacunar spinel GaV4Se8

Journal

Physical Review B, 100(4)

ISSN

2469-9950 2469-9969

Authors

Schueller, Emily C
Zuo, Julia L
Bocarsly, Joshua D
et al.

Publication Date

2019-07-23

DOI

10.1103/PhysRevB.100.045131

Peer reviewed

Modeling the structural distortion and magnetic ground state of the polar lacunar spinel GaV_4Se_8

Emily C. Schueller, Julia L. Zuo, Joshua D. Bocarsly, Daniil A. Kitchaev,
Stephen D. Wilson, and Ram Seshadri
Materials Department and Materials Research Laboratory,
University of California, Santa Barbara, Santa Barbara, CA, 93106, USA
(Dated: July 9, 2019)

The lacunar spinel GaV_4Se_8 is a material whose properties are dominated by tetrahedral clusters of V atoms. The compound is known to undergo a polar distortion to a ground state structure in the $R3m$ space group, and orders ferromagnetically with a relatively small magnetic moment. We develop an understanding into the relationship between crystal structure and magnetic order in this material, and the influence of electron correlations in establishing the observed ground state using first-principles density functional theory (DFT) electronic structure calculations. Because electrons are delocalized within V_4 clusters but localized between them, the usual approaches to simulate electron correlations — such as the use of the Hubbard U in DFT + U schemes — do not adequately recreate the experimental ground state. We find instead that the experimental ground state of GaV_4Se_8 is well-represented by the random-phase approximation to the correlation energy. Additionally, we find that magnetism and crystal structure are strongly coupled in this material, and only certain arrangements of magnetic moment within a V_4 cluster can stabilize the observed structural distortion. In combination with the anisotropic, polar nature of the material, the strength of magnetostructural coupling indicates that application of strain could be used to tune the magnetic properties of GaV_4Se_8.

I. INTRODUCTION

GaV_4Se_8 is a member of the lacunar spinel family which has garnered much attention in recent years.[1–5] The lacunar spinel structure is related to the typical AB_2O_4 spinel structure but with ordered vacancies on the A-site that induce a breathing mode distortion in the material, reducing the symmetry from $Fd\bar{3}m$ to $F\bar{4}3m$. Most significantly, the pyrochlore lattice of corner-connected tetrahedra of B-site atoms in the spinel becomes a lattice of isolated tetrahedra in the lacunar spinel. The properties of lacunar spinel materials are dominated by these clusters of transition metal atoms. For example, most exhibit a variable range hopping-type conduction, indicating electrons must hop between clusters rather than being delocalized through the material.[6] GaV_4Se_8 in particular has a small band gap at low temperature of about 0.1 eV.[4] Some members of the family, such as $GaNb_4Se_8$ and $GaTa_4Se_8$, undergo superconducting and insulator-to-metal transitions under pressure.[7,8]

GaV_4Se_8 undergoes a polar Jahn-Teller distortion along the $\langle 111 \rangle$ axis from $F\bar{4}3m$ to $R3m$ upon cooling through 41 K.[4,9] Below this temperature, at approximately 17.5 K, GaV_4Se_8 magnetically orders with an ordered moment of around $1\,\mu_B$ per cluster of four V atoms, in agreement with molecular orbital theory arguments.[4] In the magnetically ordered regime, GaV_4Se_8 hosts a rich magnetic phase diagram, with a cycloidal ground state, a skyrmion region near the ordering temperature, and a field-polarized phase at high fields.[2,3] Because of strong crystalline anisotropy along the polar $\langle 111 \rangle$ axis, the stability of phases strongly depends on the angle at which the magnetic field is applied relative to the $\langle 111 \rangle$ axis. The combination of the polar symmetry and magnetic order makes GaV_4Se_8 a multiferroic material, which could be promising for various computing and memory applications.[1]

Because magnetism, crystal structure, and electronic structure are strongly coupled in GaV_4Se_8, it can be challenging to interpret computational results. Magnetic measurements reveal a moment of $1\,\mu_B$ per tetrahedral cluster, but there are many ways this could arise, and the precise manner in which the total moment is distributed across the cluster is unclear. Furthermore, the partial delocalization of electrons in the V_4 tetrahedra is strongly dependent on electronic correlations, which are not readily modeled within density functional theory (DFT). The impact of electron correlation effects can be approximated in DFT using on-site Coulomb (U) and exchange (J) interactions which are applied to orbitals with correlated electrons, such as the d-orbitals of V. This approach is now commonly known as DFT+U,[10] and is frequently employed using a single parameter $U_{eff} = U - J$.[11] However, as we find here, GaV_4Se_8 has additional complexity because electrons can be delocalized across the four V atoms of a cluster yet remain localized to one cluster. In other words, the application of U_{eff} on individual V atoms does not capture the correct electronic ground state. The adiabatic connection fluctuation-dissipation theorem implementation of the random phase approximation (ACFDT-RPA) is a way to account for electron correlations and non-local effects in a more rigorous manner.[12] Total energy calculations with this method combine the exact exchange energy from the Hartree-Fock approximation with the correlation energy from ACFDT-RPA to provide accurate ground state predictions even for complicated materials with competing structural and magnetic ground states.[13,14]

To help lay down the basis for the computational modeling, we first prepare and measure the magnetic prop-

erties of GaV_4Se_8 single crystals. We then examine the energy landscape of GaV_4Se_8 using density functional theory calculations (with varying U_{eff} values) as well as ACFDT-RPA total energy calculations to understand the relative stability of different magnetic and structural ground states. We show that magnetism and crystal distortion are strongly coupled, and the Jahn-Teller distortion can only be stabilized with a specific arrangements of moments on the V_4-cluster. Additionally, we find that the use of ACFDT-RPA is required to recover the ground state which recreates the semiconducting behavior, elongating Jahn-Teller distortion, and net magnetic moment observed experimentally.

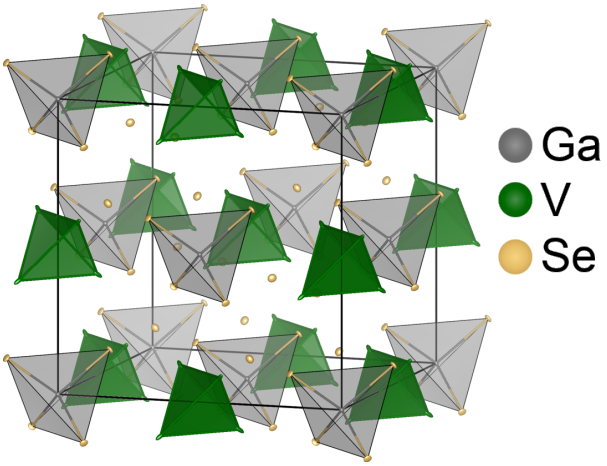

FIG. 1. The crystal structure of GaV_4Se_8 at 100 K is best fit to the expected $F\bar{4}3m$ space group from single crystal XRD. Highly anisotropic V ADPs (shown at 99%) along the axis of the low temperature Jahn-Teller distortion indicate possible local distortions of the material above the global phase transition temperature of 41 K.

II. METHODS

A. Experimental

Phase pure GaV_4Se_8 powder was obtained by reaction of Ga pieces and ground V and Se powders with an approximately 50% excess of elemental Ga. The elements were reacted in an evacuated fused silica tube with a heating ramp rate of 50° C/hour to 950° C, held for 24 h and furnace cooled. To obtain single crystals, vapor transport was performed using approximately 500 mg of the formed powder mixed with 30 mg of $PtCl_2$ as a transport agent in an evacuated fused silica tube with a diameter of 6 mm and a length close to 20 cm. The tube was held with the powder end at 960° C and the growth end at 920° C for two weeks to obtain 1-3 mg black, cuboidal, lustrous single crystals. Single crystal X-ray diffraction was performed at 100 K with a Bruker KAPPA APEX II diffractometer equipped with an APEX II CCD detector using a TRIUMPH monochromator with a Mo Kα X-ray source ($\lambda = 0.71073$ Å). Structure refinement was carried out using the Jana crystallographic computing system.[15] Crystal structures were visualized using the VESTA software suite.[16] Magnetic measurements were performed on a Quantum Design MPMS 3, with the sample mounted by attaching a crystal to a plastic drinking straw using Kapton^{TM} tape. The cuboidal shape of the crystals permitted the (100) axis of the crystal to be approximately aligned with the applied magnetic field using an optical microscope.

B. Computational

All electronic structure calculations were performed using the Vienna Ab Initio Simulation Package (VASP)[17] with the VASP recommended projector-augmented-wave pseudopotentials[18,19] within the Perdew-Burke-Ernzerhof (PBE) generalized gradient approximation (GGA).[20] PBE+U calculations were performed using the U_{eff} approach applied to the d-orbitals of V.[11] Relaxations along distortion modes were performed using selective dynamics with the conjugate gradient algorithm for ionic relaxations. For relaxations a Γ-centered K-point grid of 4×4×4 was employed. For these, a three step system was carried out in which the cell volume and ions were relaxed first, then just the ions, with Gaussian smearing with a sigma of 0.1. After the structure was relaxed, a static energy calculation was performed with the tetrahedron method with Blöchl corrections for more accurate total energy values. For band structure and density of states calculations a K-point grid of 8×8×8 was used. For the ACFDT-RPA simulations,[12] a K-point grid of 2×2×2 was used with 16 frequencies sampled (at which point the correlation energy converged within 0.1 meV/atom). For all calculations an energy cutoff of 500 eV, around 1.75 times the maximum default cutoff energy, was determined to be optimal. For the lowest and highest energy ACFDT-RPA magnetic configurations, total energy calculations were repeated with unit cell volumes changed by ±2% to confirm that the equilibrium ACFDT-RPA cell volume was close to the PBE cell volume. In order to generate structures along distortion modes, an $R3m$ structure with mode decomposition information was created with ISODISTORT[21] which contained amplitudes of distortion modes used to generate the structure from the high symmetry $F\bar{4}3m$ structure. A python script was used to systematically vary the amplitudes of chosen distortion modes (A_1 and E) and generate new structures for calculation with VASP. Calculation results were parsed and visualized with the python package pymatgen.[22] Band structure visualization employed the sumo package.[23]

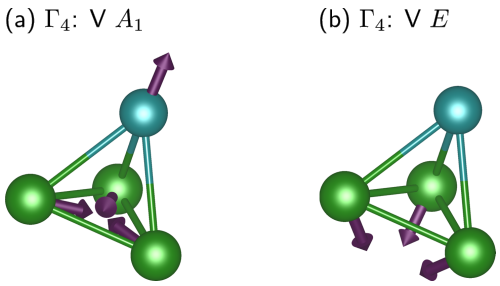

FIG. 2. The A_1 (a) and E (b) modes that distort the high symmetry (T_d) V tetrahedra into their low symmetry (C_{3v}) clusters. The V1 atom is shown in blue and the V2 atoms are shown in green.

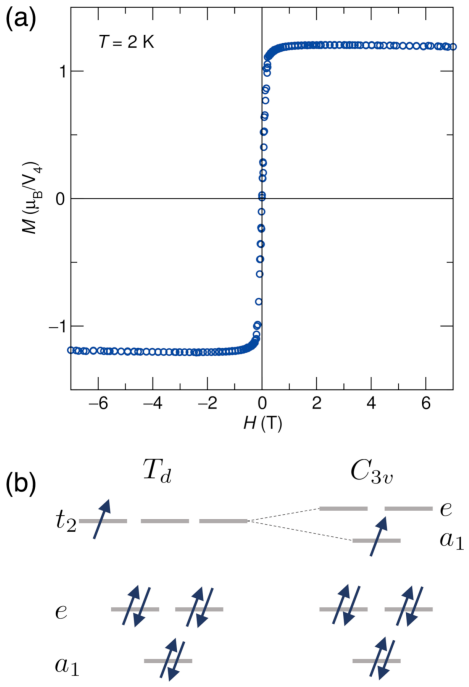

FIG. 3. (a) Field-dependent magnetization data of a GaV_4Se_8 single crystal at 2 K shows the saturation magnetization is approximately 1.1 μ_B. (b) The molecular orbital diagram of the V_4 cluster without and with the Jahn-Teller distortion (space groups changing from $F\bar{4}3m$ to $R3m$) with a net moment of 1 μ_B per V_4 cluster.

III. RESULTS AND DISCUSSION

GaV_4Se_8 has a molecules-in-crystal structure with isolated tetrahedral clusters of transition metal atoms, as shown in Fig. 1, a structure fit from high resolution single crystal X-ray diffraction (XRD) measurements taken at 100 K. From molecular orbital theory, it is expected that in the high temperature phase, the cluster has T_d symmetry with one electron in the t_2 orbital, making it unstable to a Jahn-Teller distortion. In GaV_4Se_8, this distortion occurs around 41 K along the $\langle 111 \rangle$ direction, lowering the structural symmetry to $R3m$.[4] This makes one V atom on the cluster (V1, shown in blue in Fig. 2) inequivalent from the other three (V2, shown in green in Fig. 2). Even in the high temperature, nominally cubic phase, the single crystal XRD refinement on 100 K data indicates V atomic displacement parameters which are highly anisotropic and point along the $\langle 111 \rangle$ directions, indicating local Jahn-Teller distortions are likely present above the global phase transition temperature.[24,25] The measured saturation magnetization of GaV_4Se_8 is 1.1 μ_B per V_4 cluster as shown in Fig. 3(a). Following the Jahn-Teller distortion, the cluster has C_{3v} symmetry, splitting the degenerate t_2 into a half-filled a_1 orbital and an empty e orbital, as shown in Fig. 3(b).[9] Molecular orbital theory yields a moment of 1 μ_B per V_4, matching what is measured in experiment.

In order to more fully understand the unusual structural and magnetic properties GaV_4Se_8, we wished to probe the underlying physics governing the magnetic and structural ground state, as well as investigate the distribution of moment across the pseudo-tetrahedral cluster of V atoms which is difficult to study experimentally. To do this, we performed density functional theory calculations in VASP using the PBE functional. We began with a typical magnetic initialization of 3 μ_B per V atom, but found that this resulted in a relaxed structure with a moment of around 5 μ_B per cluster, far higher than the experimental and molecular orbital theory predicted values. Because in the $R3m$ structure, one V is inequivalent from the other 3 in the cluster, there are several possible collinear arrangements of moments that are compatible with the space group symmetry. We focus on three possible magnetic configurations: the previously mentioned high moment configuration, which we will call HFM, a ferrimagnetic configuration where the inequivalent V1 is spin up and the three V2 are spin down, which we will call FI1 if it is accompanied by a compressive structural distortion and FI2 if the accompanying distortion is elongative, and a low moment configuration where the moment on each V is initialized to 0.5 μ_B, which we will call LFM. We find that the crystal distortion is strongly coupled to the magnetic configuration, and the reported low temperature experimental structure is *not* the most stable structure for all of the magnetic configurations. Because all of these variables are highly correlated, a systematic approach is required to obtain a full picture of the energy landscape.

Starting from the high symmetry $F\bar{4}3m$ structure, group theory can be used to generate linearly independent sets of vectors (distortion modes) that the atoms follow from their high symmetry positions to their positions in the lower symmetry $R3m$ structure. The full transformation from the $F\bar{4}3m$ to $R3m$ unit cell for GaV_4Se_8 has ten linearly independent displacive modes, but we focus on the two that affect the motion of the V atoms, A_1 and E, because the V atoms control the magnetism and contribute the most to the band structure around the Fermi energy. These modes, illustrated in Fig.2 (a) and (b) respectively, distort the shape of the tetrahedron and

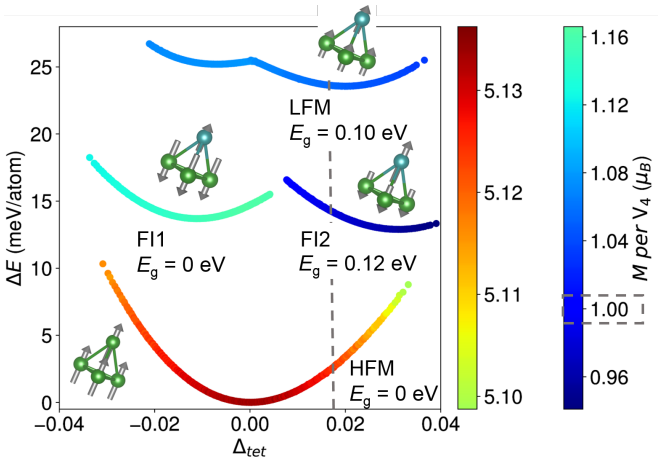

FIG. 4. The calculated energy landscape within PBE for GaV_4Se_8 versus tetrahedral distortion with $U = 0\,eV$. The arrows on the tetrahedra are representative magnetic structures, which are accompanied by text labels, for each parabola and the colors of the atoms represent their structural equivalence. The colors of the parabolas are the net moment for each structure. The dashed grey lines represent experimentally observed values of Δ_{tet} and net moment. The ground state structure (HFM) within PBE has a far higher net magnetic moment than the experimentally observed value.

translate it within the unit cell. When the amplitudes of both modes are 0, this generates a perfect tetrahedron, corresponding to the undistorted, cubic phase. The amplitudes of these two modes are systematically varied to generate structures with an array of different shapes and positions of the V cluster within the unit cell.

These structures are simulated with VASP to understand the coupling between the shape of the tetrahedron and the energies of various magnetic configurations. In order to isolate these modes we fix the positions of the V atoms within the structure and relax other ion positions as well as lattice parameters and cell shape. However, in doing so we remove the translation effect of the A_1 and E modes, and therefore their independence. To reduce the dimensionality of the analysis, we combine the effect of the two modes into a tetrahedral distortion parameter which is a difference of bond lengths between V1 and V2 and between V2 and V2:

$$\Delta_{tet} = \frac{d_{[V1-V2]} - d_{[V2-V2]}}{d_{[V1-V2]} + d_{[V2-V2]}}$$

Within PBE and without any effort to correct for electron correlation, we find the energy landscapes shown in Fig. 4. The high moment configuration (HFM, 5 μ_B/V_4) is found to be the most stable for all distortions of the tetrahedral cluster. Structurally, this magnetic configuration has an energetic minimum at no tetrahedral distortion, with the unit cell relaxing to the high temperature $F\bar{4}3m$ structure. Additionally, it has a metallic band structure, unlike the experimental semiconducting behavior, which is unsurprising given the small degree of structural distortion. Therefore, we see that the ground state calculated by PBE alone does not reproduce the electronic, crystal structure, or magnetic behavior observed in experiment.

The two higher energy parabolas (around 10 meV/atom higher in Fig. 4) represent magnetic structures with ferrimagnetic configurations on the cluster (FI1 and FI2). On the right side, there is a ferrimagnetic state with a strong moment on V1 and weak opposing moments on V2 (FI2). This magnetic configuration couples with an elongative Jahn-Teller distortion where the V1 atom is far from V2 and V2 are close to each other (as in the experimental structure). On the left side, the Jahn-Teller distortion is compressive with V1 close to the V2 and V2 pushed farther from each other. The ferrimagnetic state created, FI1, has a weaker moment on V1 and stronger opposing moments on V2. The FI2 configuration on the right side (elongative Jahn-Teller) has a small band gap, while the left side (FI1) configuration is gapless. Finally, the highest energy parabolas are low moment ferromagnetic configurations with a 1 μ_B moment essentially delocalized across each cluster. The minimum on the right side (LFM) is again gapped. This high energy configuration agrees most closely with the experimental crystal distortion, net magnetic moment, and band gap. Therefore, without accounting for electron correlations, we obtain a metallic ground state with a nearly cubic structure and a large moment.

Since V is a $3d$ atom, it is not surprising that it may be necessary to account for electron correlations; for example, in the form of a Hubbard U, which promotes electron localization on specific V d-orbitals, to correctly represent the ground state of a V-containing compound. We repeated the systematic generation of an energy landscape for increasing values of U_{eff} within PBE. Energy landscapes for U_{eff} = 0.9 eV and U_{eff} = 3 eV are shown in Fig. 5. While a value for U_{eff} of 3 eV stabilizes a gapped ground state, the Jahn-Teller distortion occurs in the opposite direction (compressing rather than elongating along the $\langle 111 \rangle$ axis) to what is observed in experiment, and the net moment is 8 μ_B/V_4, which is far higher than the experimentally observed value. Additionally, the increase of U_{eff} destabilizes other magnetic configurations relative to the high moment configuration, presumably since these other configurations have lower moments, indicating the spins are more delocalized across the cluster. Therefore, PBE+U_{eff} does not adequately capture the behavior of this cluster compound. We speculate that the reason for the failure of the Hubbard U correction is that the true electronic configuration of the V_4 cluster is best described by a molecular orbital picture, with the low-spin ferromagnetic state controlled by $d-d$ hopping rather than conventional double exchange. Following the description given by Streltsov and Khomskii[26], this mechanism requires the redistribution of electrons away from localized d-orbitals, and into molecular orbitals formed by covalent metal-metal

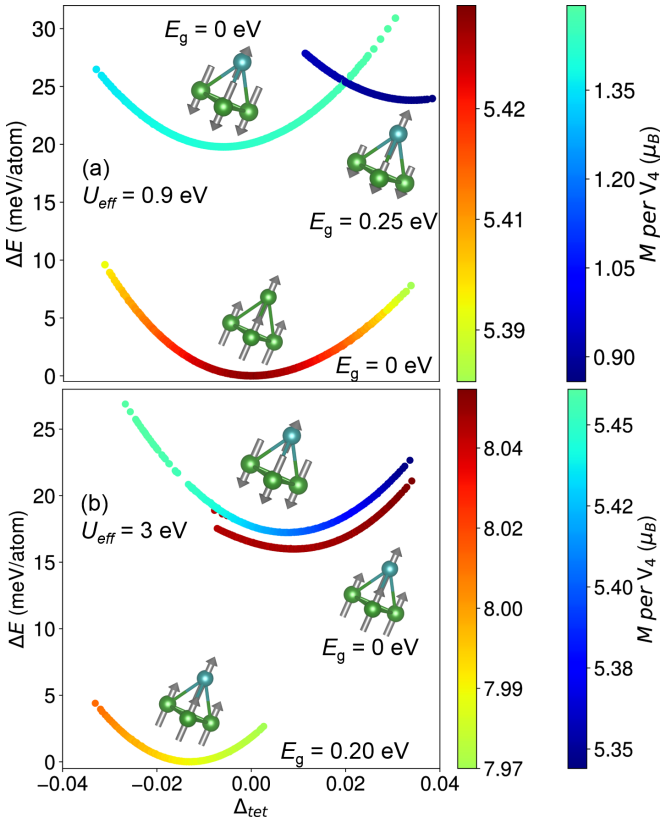

FIG. 5. The calculated energy landscape for GaV_4Se_8 versus tetrahedral distortion at (a) U_{eff} = 0.9 eV and (b) U_{eff} = 3 eV. The arrows on the tetrahedra are representative magnetic structures for each parabola and the colors of the atoms represent their structural equivalence. The colors of the parabolas indicate the net moment for each structure. Increasing values of U destabilize configurations with low net moments relative to high net moment configurations, as expected due to increasing localization of electrons on the V atoms.

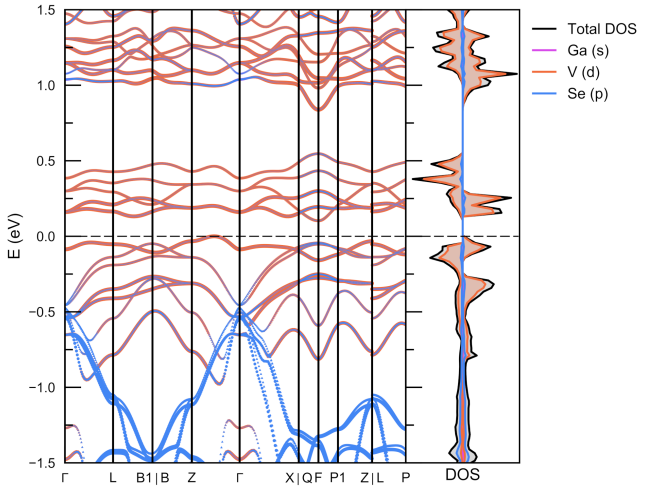

FIG. 6. Spin-polarized band structure and densities of state from PBE calculations for what is established by ACFDT-RPA as the ground state, with a low net magnetic moment, ferromagnetic distribution of moment across a cluster, and an elongative Jahn-Teller distortion. The structural and magnetic energetics of this calculation correspond to the LFM minimum in Fig. 4.

bonds. The addition of an on-site Hubbard U suppresses this redistribution and thus leads to worse results than pure PBE.

A more sophisticated approach to account for electron correlations is ACFDT-RPA,[12] which enabled total energy calculations using exact exchange energies from Hartree-Fock with correlation corrections. This method has been successfully employed to obtain the correct experimental ground state in other materials with competing ground states, including correlated magnetic materials.[13,14] The Kohn-Sham orbitals from the PBE ($U = 0$ eV) low moment ferromagnetic (LFM) and ferrimagnetic (FI1 and FI2) minima along with the high moment (HFM) PBE ground state were selected as a starting point for ACFDT-RPA calculations. Table I shows a comparison of the ACFDT-RPA and PBE total energies for the four magnetic configurations (called LFM, FI1, FI2, and HFM respectively), as well as a breakdown into exchange and correlation energies for the ACFDT-RPA calculations. ACFDT-RPA stabilizes the LFM configuration, which has a net moment, crystal structure, and band gap similar that are close to the experimental values. As seen in Table I, the HFM configuration is significantly more stable for the exchange energy, but correlation stabilizes the LFM configuration. The inability of PBE, even with a Hubbard U correction, to find the correct ground state is due to inadequate treatment of correlation energies in materials where the electronic structure is more adequately described with molecular orbitals rather than atomic orbitals.

Since ACFDT-RPA establishes the lowest-energy state as the one corresponding to a low-moment, ferromagnetic distribution of moment across a cluster with an elongative Jahn-Teller structure, the corresponding spin-polarized PBE band structure and densities of state are displayed in Fig. 6. A gap close to 0.1 eV is seen, which is similar to what has been reported from the low-temperature hopping conductivity measurements.[4] The valence and conduction states have largely V d-orbital character, and the molecular nature of the lacunar spinel crystal structure ensures relatively narrow dispersion of the bands.

Figure 7 highlights the effectiveness of the ACFDT-RPA approach to modeling electron correlation effects compared with traditional PBE and PBE with U_{eff} approaches. Particularly, ACFDT-RPA succeeds in reproducing experimentally observed magnetic and electronic properties as well as crystal structure distortion. The ground state from the ACFDT-RPA method is the only one which has an elongative Jahn-Teller distortion (shown as a positive value of Δ_{tet}) and a net magnetic moment close to the 1 μ_B per V_4 expected from group theory and verified in experiment.

TABLE I. Comparison of PBE and ACFDT-RPA energies for different magnetic and structural configurations. ΔE is referenced to the lowest energy in the sequence of calculations.

state	exchange (eV)	correlation (eV)	total (eV)	ΔE (meV atom^{-1})	total (eV)	ΔE (meV atom^{-1})
	ACFDT-RPA				PBE	
high (HFM)	−164.26	−173.86	−338.12	24.49	−76.41	0
elongative ferri (FI2)	−161.31	−176.98	−338.29	11.21	−76.25	12.99
compressive ferri (FI1)	−161.07	−177.31	−338.38	4.18	−76.24	13.56
low (LFM)	−158.05	−180.38	−338.44	0	−76.10	23.97

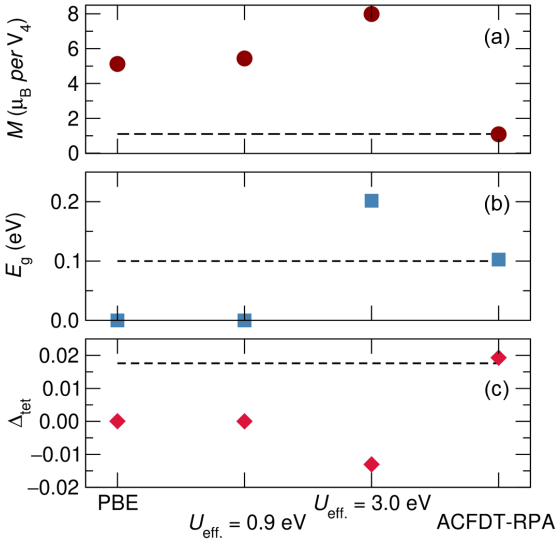

FIG. 7. Ground state net magnetic moment (a), band gap (b), and tetrahedral distortion (c) for DFT calculations performed with varying levels of electron correlation corrections. The ground state established by ACFDT-RPA shows the greatest agreement with the experimental values (shown as dashed lines) for the magnetic, electronic, and crystal structure properties as compared to the ground states from PBE and PBE+U_{eff}.

IV. CONCLUSIONS

In GaV_4Se_8, the magnetic behavior is described by a hierarchy of magnetic interactions: the size of the atomic moments, the nature of intra-cluster and inter-cluster interactions, and additionally, the coupling between structural distortions and magnetic configurations. While the inter-cluster magnetic interactions have been probed experimentally,[1,2,4] intra-cluster interactions are harder to resolve. In a system where magnetism and crystal structure are strongly coupled, group theory can be a powerful tool to systematically explore the energy landscape. In combination with DFT, group theory allows us to consistently elucidate the couplings between structural and magnetic degrees of freedom in this system. Only certain magnetic configurations can support a Jahn-Teller distortion in GaV_4Se_8, and different configurations stabilize different distortions of the crystal structure, indicating strong magnetostructural coupling. This relationship, in addition to the crystal anisotropy from the polar space group, suggests that the application of strain will allow for the manipulation of magnetism in GaV_4Se_8. Additionally, in compounds with clusters of atoms, magnetism and electron correlation effects must be carefully considered. In such systems, more sophisticated approaches than DFT+U, such as ACFDT-RPA, may be required to obtain the correct energy landscape.

ACKNOWLEDGMENTS

We thank Dr. Matthew Horton for help in generating distorted structures and Nicholas Wagner for useful comments on the manuscript. This research was supported by the National Science Foundation (NSF) through the DMREF program DMR 1729489. Partial support from the Materials Research Science and Engineering Center (MRSEC) at UC Santa Barbara to D. A. K. through NSF DMR 1720256 (IRG-1) is gratefully acknowledged, as is use of the shared facilities of the MRSEC. The UCSB MRSEC is a member of the NSF-supported Materials Research Facilities Network (www.mrfn.org). We also acknowledge support from the Center for Scientific Computing at UC Santa Barbara supported by NSF DMR-1720256 and NSF CNS-1725797.

[1] E. Ruff, A. Butykai, K. Geirhos, S. Widmann, V. Tsurkan, E. Stefanet, I. Kezsmarki, A. Loidl, and P. Lunkenheimer, Phys. Rev. B **96**, 165119 (2017).
[2] Y. Fujima, N. Abe, Y. Tokunaga, and T. Arima, Phys. Rev. B **95**, 180410 (2017).
[3] S. Bordacs, A. Butykai, B. G. Szigeti, J. S. White, R. Cubitt, A. O. Leonov, S. Widmann, D. Ehlers, H.-A. K. von Nidda, V. Tsurkan, A. Loidl, and I. Kezsmarki, Sci. Rep. **7**, 7584 (2017).
[4] D. Bichler, *Magnetismus und strukturelle Phasenumwandlungen von Verbindungen mit tetraedrischen Metallclustern*, Ph.D. thesis, Ludwig-Maximilians-Universitat Munchen (2010).
[5] D. Bichler and D. Johrendt, Chem. Mater. **23**, 3014 (2011).

[6] Y. Sahoo and A. K. Rastogi, J. Phys.: Condens. Matter **5**, 5953 (1993).
[7] R. Pocha, D. Johrendt, B. Ni, and M. M. Abd-Elmeguid, J. Am. Chem. Soc. **127**, 8732 (2005).
[8] A. Camjayi, C. Acha, R. Weht, M. G. Rodríguez, B. Corraze, E. Janod, L. Cario, and M. J. Rozenberg, Phys. Rev. Lett. **113**, 086404 (2014).
[9] R. Pocha, D. Johrendt, and R. Pottgen, Chem. Mater. **12**, 2882 (2000).
[10] A. I. Liechtenstein, V. I. Anisimov, and J. Zaanen, Phys. Rev. B **52**, R5467 (1995).
[11] S. L. Dudarev, G. A. Botton, S. Y. Savrasov, C. J. Humphreys, and A. P. Sutton, Phys. Rev. B **57**, 1505 (1998).
[12] J. Harl and G. Kresse, Phys. Rev. Lett. **103**, 056401 (2009).
[13] H. Peng and S. Lany, Phys. Rev. B **87**, 174113 (2013).
[14] L. Schimka, R. Gaudoin, J. Klimes, M. Marsman, and G. Kresse, Phys. Rev. B **87**, 214102 (2013).
[15] V. Petricek, M. Dusek, and L. Palatinus, Z. Kristallogr. Cryst. Mater. **229**, 345 (2014).
[16] K. Momma and F. Izumi, J. Appl. Crystallogr. **44**, 1272 (2011).
[17] G. Kresse and J. Furthmuller, Phys. Rev. B **54**, 11169 (1996).
[18] P. E. Bloch, Phys. Rev. B **50**, 17953 (1994).
[19] G. Kresse and D. Joubert, Phys. Rev. B **59**, 1758 (1999).
[20] J. P. Perdew, K. Burke, and M. Ernzerhof, Phys. Rev. Lett. **77**, 3865 (1996).
[21] B. J. Campbell, H. T. Stokes, D. E. Tanner, and D. M. Hatch, J. Appl. Cryst. **39**, 607 (2006).
[22] S. P. Ong, W. D. Richards, A. Jain, G. Hautier, M. Kocher, S. Cholia, D. Gunter, V. L. Chevrier, K. A. Persson, and G. Ceder, Comput. Mater. Sci. **68**, 314 (2013).
[23] A. M. Ganose, A. J. Jackson, and D. O. Scanlon, J. Open Source Softw. **3**, 717 (2018).
[24] T. Proffen, R. G. DiFrancesco, S. J. L. Billinge, E. L. Brosha, and H. G. Kwei, Phys. Rev. B **60**, 9973 (1999).
[25] D. P. Shoemaker, J. Li, and R. Seshadri, J. Am. Chem. Soc. **131**, 11450 (2009).
[26] S. V. Streltsov and D. I. Khomskii, Proc. Natl. Acad. Sci. **113**, 10491 (2016).